AGU PUBLICATIONS

Water Resources Research

RESEARCH ARTICLE
10.1002/2016WR019258

Evaporation fractionation in a peatland drainage network affects stream water isotope composition

Matthias Sprenger [1], Doerthe Tetzlaff [1], Claire Tunaley [1], Jonathan Dick[1], and Chris Soulsby[1]

[1]Northern Rivers Institute, School of Geosciences, University of Aberdeen, Aberdeen, UK

Key Points:
- Kinetic isotopic fractionation in peatland drainage correlates positively with potential evapotranspiration and negatively with discharge
- The interplay between the precipitation, evaporation, hydrologic connectivity, and groundwater explains the isotopic fractionation signal
- The isotopic enrichment within the peatland drainage network is imprinted on the stream water

Supporting Information:
- Supporting Information S1

Correspondence to:
M. Sprenger,
matthias.sprenger@abdn.ac.uk

Citation:
Sprenger, M., D. Tetzlaff, C. Tunaley, J. Dick, and C. Soulsby (2017), Evaporation fractionation in a peatland drainage network affects stream water isotope composition, *Water Resour. Res.*, *53*, 851–866, doi:10.1002/2016WR019258.

Received 23 MAY 2016
Accepted 27 NOV 2016
Accepted article online 15 DEC 2016
Published online 25 JAN 2017

Abstract There is increasing interest in improving understanding of evaporation within a catchment for an enhanced representation of dominant processes in hydrological models. We used a dual-isotope approach within a nested experimental design in a boreal catchment in the Scottish Highlands (Bruntland Burn) to quantify the spatiotemporal dynamics of evaporation fractionation in a peatland drainage network and its effect on stream water isotopes. We conducted spatially distributed water sampling within the saturated peatland under different wetness conditions. We used the lc-excess—which describes the offset of a water sample from the local meteoric water line in the dual-isotope space—to understand the development of kinetic fractionation during runoff in a peatland network. The evaporation fractionation signal correlated positively with the potential evapotranspiration and negatively with the discharge. The variability of the isotopic enrichment within the peatland drainage network was higher with higher potential evapotranspiration and lower with higher discharge. We found an increased evaporation fractionation toward the center of the peatland, while groundwater seepage from minerogenic soils influenced the isotopic signal at the edge of the peatland. The evaporation signal was imprinted on the stream water, as the discharge from a peatland dominated subcatchment showed a more intense deviation from the local meteoric water line than the discharge from the Bruntland Burn. The findings underline that evaporation fractionation within peatland drainage networks affects the isotopic signal of headwater catchments, which questions the common assumption in hydrological modeling that the isotopic composition of stream waters did not undergo fractionation processes.

1. Introduction

The temporal and spatial assessment of evaporation within different landscape units remains unresolved, but knowledge about such process variation within catchments has been shown to help calibrate and benchmark rainfall-runoff models [*Birkel et al*., 2014; *Anderton et al*., 2002]. In particular, where models also incorporate solute transport and mixing, constraining, and calibrating evaporation estimates and their consequent influence on tracer dynamics is especially challenging. Evaporation alters the isotopic composition in surface waters, which are often used to infer mixing and derive travel time estimates [*McGuire and McDonnell*, 2006]. However, for travel time studies, evapotranspiration losses may be crucial to assess the temporal variability of hydrological fluxes [*Soulsby et al*., 2016; *Sprenger et al*., 2016b]. The age distribution of evapotranspiration (the "evapotranspiration time" [*Botter et al*., 2010]) is increasingly considered [*van Huijgevoort et al*., 2016; *Harman*, 2015; *Soulsby et al*., 2015; *Queloz et al*., 2015]. Evaporation induces kinetic fractionation of the composition of stable isotopes of the residual water [*Craig et al*., 1963], while transpiration does not change the isotope signal of the water remaining in the catchment [e.g., *Zimmermann et al*., 1967; *Allison et al*., 1984]. Thus, for waters that experienced evaporation losses, the relation between $\delta^{18}O$ and $\delta^{2}H$ deviates from the original isotopic composition of precipitation. The original isotopic composition is characterized for surface waters by the local meteoric water line (LMWL), which describes the $\delta^{18}O$-$\delta^{2}H$ ratio for the rainfall. Water that experienced evaporation fractionation will plot below the LMWL; as, for example, observed in streams draining lakes [e.g., *Gibson and Reid*, 2010; *Gibson and Edwards*, 2002; *Isokangas et al*., 2015] or beaver ponds [*Burns and McDonnell*, 1998]. However, a recent global analysis of the isotopic signal in the discharge of headwater catchments in tropical, subtropical, and temperate regions. *Evaristo et al*. [2015] found that the stream water does usually not show signs of evaporation fractionation. As such, traditional assumptions that catchment outflows do not reflect isotopic fractionation seem to hold for many

of the headwater catchments in these regions. However, sites from northern latitudes were not included in *Evaristo et al*. [2015]. It is known that peatlands in these areas, defined as rain-fed (ombrotrophic) bog, groundwater-fed (minerotrophic) fen, or a combination of both (bog-fen complex) [*Gore*, 1983], generally increase the evaporation losses [*Bullock and Acreman*, 2003]. Consequently, pronounced evaporation fractionation signals have been found in pools of peatland drainage networks in boreal headwater catchments [*Carrer et al*., 2016; *Gibson et al*., 2000]. Nevertheless, the temporal variation of these evaporation fractionation processes in headwater catchments with peatland drainage networks and the environmental drivers of these processes remain poorly understood. Especially, if and when the fractionation is passed on to the stream network is yet unknown. A consideration of these evaporation fractionation processes in peatland drainage networks is a critical prerequisite for an accurate representation of the hydrological fluxes and to infer catchment travel times.

For the northern upland catchment of the Bruntland Burn in Scotland, *Birkel et al*. [2011] showed that adding evaporation fractionation in the water-saturated areas into their hydrological model based on the Craig-Gordon Model [*Craig and Gordon*, 1965] improved the simulation of the isotopic signal in the stream water. However, even the additional inclusion of fractionation in the unsaturated soil led to an underestimation of the isotopic fractionation during summer periods [*Birkel et al*., 2014]. Therefore, we know that evaporation fractionation plays a role in the isotopic composition of runoff generated from the Bruntland catchment, but we do not have an understanding of when, where, and in which way the isotopically enriched water feeds the stream.

Thus, the objectives of our study are (i) to investigate stable isotope dynamics in a northern upland catchment, (ii) to quantify spatiotemporal dynamics of evaporation fractionation in a peatland drainage network, and (iii) to assess the effect of spatially distributed fractionation on the stream water signature.

2. Study Site

The study was conducted in the 3.2 km^2 Bruntland Burn (BB) experimental catchment, a tributary of the Girnock Burn, in the Scottish Highlands (57°02′18.4″N 3°07′52.0″W). The catchment has been the focus of numerous hydrological studies to which the reader is referred to for a detailed description [e.g., *Blumstock et al*., 2015; *Tetzlaff et al*., 2014; *Soulsby et al*., 2015]. The temperate/boreal oceanic climate is characterized by a mean annual air temperature of 7°C and 1000 mm yr^{-1} of mean annual precipitation. Usually, less than 5% and maximum of 10% of the precipitation fall as snow [*Soulsby et al*., 2015]. While the temperature varies seasonally with daily means of 2°C in January and 13°C in July, the rainfall shows a less marked seasonal pattern and is fairly evenly distributed throughout the year. The annual evapotranspiration (*ET*) is about 400 mm yr^{-1}, mostly occurring between May and August.

The geology of the BB is dominated by granitic bedrock in the north and metamorphic bedrock in the south. Above the low permeability bedrock, glacial deposits and till of varying depths from 5 m on the hillslopes to 40 m in the valley bottom, cover up to 70% of the catchment. These drift deposits have a relatively low hydraulic conductivity (10^{-6}–10^{-4} m s^{-1}) and form the main source of groundwater storage [*Soulsby et al*., 2015].

The soils that have developed on the drift deposits differ according to the topography. On the hillslopes, freely draining shallow (<0.7 m) podzols and rankers are predominant. In the valley bottom, deep soils (>1 m) rich in organic material classified as peats and peaty gleys prevail (Figure 1). The peat covers about 9% of the BB, mostly in riparian areas fringing the main stream channel. Peaty gleys are also found in the riparian zone, but where slopes are slightly higher, and cover 10% of the total catchment area. The peat is permanently at, or close to, saturation and the groundwater table is always within 0.25 m below the surface, while the groundwater level can drop deeper than this (to ~0.4 m) during very dry conditions in the peaty gleys [*Blumstock et al*., 2016]. The extension of fully saturated soils in the BB was found to be 2–40% depending on antecedent wetness conditions during the field surveys [*Birkel et al*., 2010]. The peat soils are characterized by a complex peatland drainage network on the surface resulting in fill-and-spill runoff mechanisms [*Spence and Woo*, 2003]: Due to the low hydraulic conductivity in the deeper, more humified peat, water movement is mostly lateral in the upper 0.2 m of poorly humified peat (acrotelm). Drainage from this horizon in the larger soil pores collects in small zero order channels which often drain through networks of small interconnected ponds [*Tetzlaff et al*., 2014; *Lessels et al*., 2016]. The peatland drainage network is also

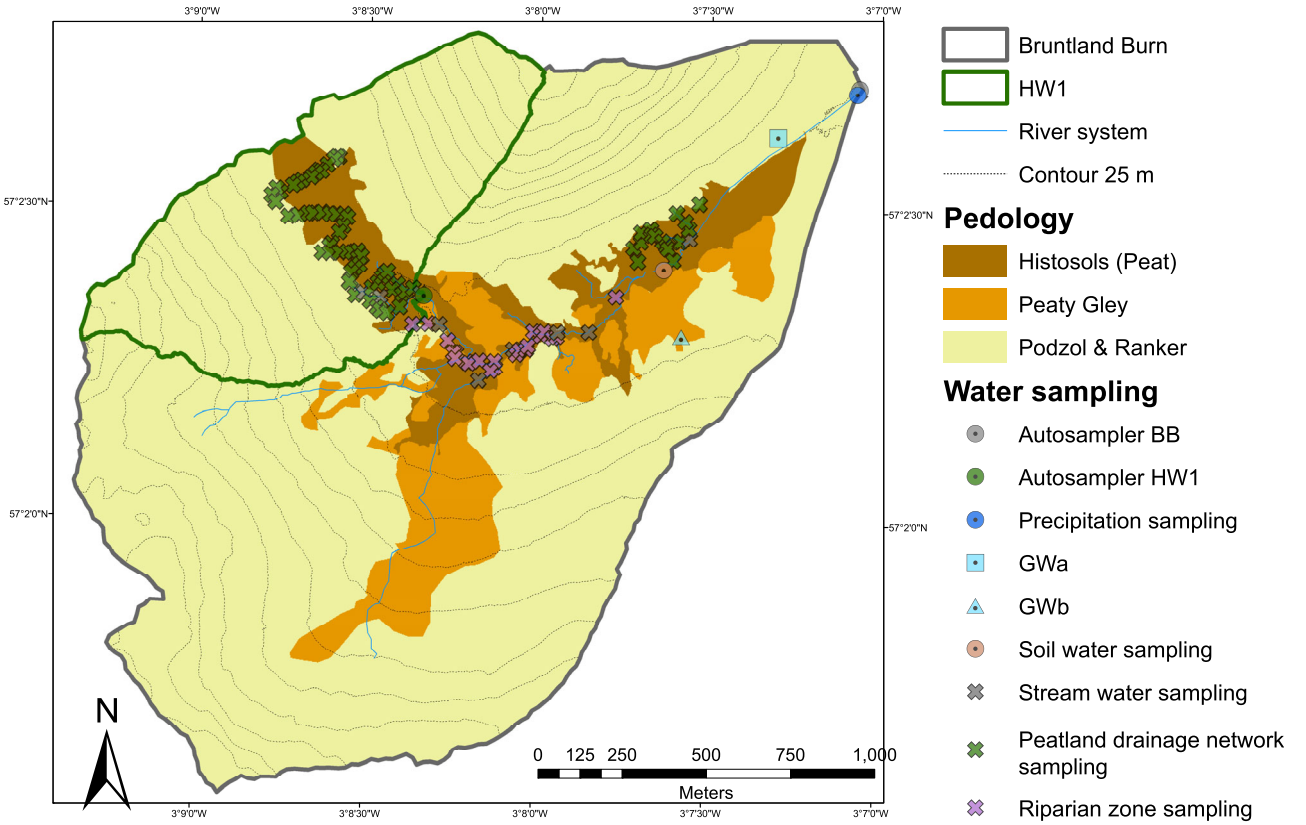

Figure 1. The Bruntland Burn catchment and its distribution of soil types. The green line shows the boundary of the HW1 subcatchment. Sampling locations are shown for rainfall, stream water at the outlet of HW1 and the Bruntland Burn (BB), groundwater, mobile soil water, and spatially distributed sampling of open surface waters in the peatland drainage network, the riparian zone, and stream water.

fed by minerogenic groundwater seepage at the edges. Toward the center, where the peat accumulates to a raised bog, ombotrophic (rain-fed) conditions prevail. This way, the peatland drainage network represents as a bog-fen complex a continuum integrating groundwater and soil water, then flowing along shallow water tracks and pools.

For our study, we used a nested experimental design, where we monitored a 0.73 km^2 headwater catchment (HW1) of the BB (green boundaries in Figure 1). HW1 is characterized by an extensive raised peat bog [*Blumstock et al.*, 2015; *Dick et al.*, 2015]. The bog is surrounded by a groundwater-fed fen area, receiving groundwater seepage from the surrounding steep hillslopes [*Lessels et al.*, 2016]. Peat soils cover 14% of HW1. Overall, we could distinguish four different landscape units (Figure 1): the total BB, the subcatchment HW1, the peatland drainage network, defined as the extended raised peatland (bog) with dynamically connected/disconnected drainage networks, and the riparian zone of the BB, where the drainage network is more continuously connected and the contribution of minerogenic drainage from the hillslopes is higher. The locations of the water sampling for each unit are shown in Figure 1.

The vegetation on the peatland drainage network is dominated by *Sphagnum* spp. mosses along the water tracks and pools. In the riparian zone of the BB, minerogenic drainage from the hillslopes allow *Molinia caerulea* grasses to compete with *Sphagnum* Mosses. On the rankers and podzols, heather (*Calluna vulgaris* and *Erica* spp.) is the dominant shrub, while trees (mainly *Pinus sylvestris*) are mostly limited to the hillslopes covering only 10% of the BB. However, heavy grazing of Red Deer (*Cervus elaphus*) prevents the development of a forest cover on the steep hillslopes.

3. Data and Methods

The study spanned the period from 1 June 2011 to 31 December 2015. Meteorological data (precipitation, net radiation, air temperature, relative humidity) were collected at 15 min intervals 1 km away from the BB

outlet by Marine Scotland Science. Based on this data, daily potential evaporation (*PET*) was estimated using the Penman-Monteith equation. To account for the local vegetation characteristics, the aerodynamic and canopy roughness parameters were adjusted to the local conditions in the Scottish Highlands as suggested by *Dunn and Mackay* [1995]. While the absolute values will vary depending on the aerodynamic and canopy roughness parameters, the temporal dynamics, which are of relevance for our analysis, are not affected by the parameter choice. In our analysis, we use *PET* as a measure for the potential evaporation without an arbitrary partitioning between evaporation and transpiration, since the evaporation and the transpiration are found to have a linear relation in temperate climates [*Renner et al*., 2016; *Schwärzel et al*., 2009]. The daily discharge at the BB outlet was derived from 15 min stage height records (Odyssey capacitance probe, Christchurch, New Zealand) in a stable, rated stream section. Water levels were translated into discharge by a rating curve ($y = 4E-10x^{5.2119}$) based on at least monthly gaugings in the years 2011 and 2012 and event-based gauging since then to address bias toward base flows. Stream water at the outlets of both HW1 (from May 2014 onward) and BB as well as rainfall were sampled on daily basis using ISCO 3700 (Teledyne Isco, Lincoln, USA) automatic water samplers (locations indicated in Figure 1). To avoid sample evaporation, paraffin was added to the autosampler bottles and the bottles were emptied in at least a fortnightly frequency. Soil water was extracted weekly until November 2013 from a peat soil (for location see Figure 1) at −10 and −30 cm depth by applying a vacuum to Rhizon soil moisture samplers (Rhizosphere Research Products, Wageningen, Netherlands) [*Tetzlaff et al*., 2014]. Suction lysimeters, like the Rhizon sampler, were shown to sample the mobile soil water in a comparison with other soil water isotope methods [*Sprenger et al*., 2015]. Two groundwater springs draining deeper groundwater stores (>5 m depth) were sampled fortnightly until May 2012 (GWa and GWb in Figure 1) [*Birkel et al*., 2011].

The drainage network of channels and pools in the valley bottom of the BB was sampled at up to 94 locations on six sampling days between September 2011 and September 2013. The sample number varied between 35 and 94, since the sampling days cover different catchment wetness states. These spatially distributed samples were divided into a dynamically connected/disconnected peatland drainage network (green crosses in Figure 1) and more perennially connected waters of the riparian zone (purple crosses in Figure 1). In parallel to the spatially distributed sampling, stream water was sampled at 10 different locations along the perennial main stream (grey crosses in Figure 1).

All samples were stored in air tight vials and kept refrigerated until they were analyzed for their water stable isotopic composition with a Los Gatos DLT-100 laser isotope analyzer (Los Gatos Research, Inc., San Jose, USA). The precision of the measurements is given as $\pm 0.1‰$ for oxygen-18 ($\delta^{18}O$) and $\pm 0.4‰$ for deuterium ($\delta^{2}H$). The isotopic composition is given in the delta notation (in ‰) describing the relative difference in the ratio of heavy to light isotopes of a water sample to the Vienna Standard Mean Ocean Water (VSMOW).

The isotopic composition of precipitation is characterized by equilibrium fractionation processes leading to a strong correlation between $\delta^{18}O$ and $\delta^{2}H$ in rainfall water (Global Meteoric Water Line, GMWL, *Dansgaard* [1964]). This relation is described locally by the local meteoric water line (LMWL) representing the regression line, characterized by a slope and a $\delta^{2}H$-axis intercept, between $\delta^{18}O$ and $\delta^{2}H$ in a dual-isotope plot (LMWL for the BB: $\delta^{2}H = 7.7 \times \delta^{18}O + 5.1$). However, since the heavier $^{1}H_{2}^{18}O$ isotopologue (molecular weight = 20.015 g mol^{-1}) [*Horita et al*., 2008] is less likely to change from the liquid phase to the gaseous phase than the lighter $^{1}H^{2}H^{16}O$ isotopologue (molecular weight = 19.017 g mol^{-1}) [*Horita et al*., 2008], the ratio between $\delta^{18}O$ and $\delta^{2}H$ will change during evaporation processes, called kinetic fraction processes [*Craig et al*., 1963]. As a result, water samples that experienced evaporation will plot below the LMWL. As more water evaporates, the remaining water from which the evaporation takes place gets more kinetically fractionated. These samples will increasingly deviate from the LMWL and their regression line in the dual-isotope plot will have a slope that is lower than the LMWL. This regression line is usually called evaporation water line (EWL). The resulting deviation of the water sample from the LMWL is described as the line-conditioned excess (lc-excess) as defined by *Landwehr and Coplen* [2006]:

$$lc\text{-}excess = \delta^{2}H - a \times \delta^{18}O - b\,, \qquad \text{(Eq. 1)}$$

with a and b representing the slope and intercept of the LMWL (for BB: $a = 7.7‰$; $b = 5.1‰$). While the widely applied deuterium-excess (d-excess) [*Dansgaard*, 1964] describes the offset between the $\delta^{2}H$ of a water sample on the GMWL to a water sample in the dual-isotope space at a given $\delta^{18}O$, the lc-excess uses the LMWL as reference. We derived for our water samples the lc-excess and their uncertainty was estimated based on the precision of the isotope analysis and the slope of the LMWL to be $\pm 1.17‰$.

We computed 14 days mean lc-excess of *P* ($lc\text{-}excess_{P14}$) and daily *PET* (PET_{14days}) to account for the antecedent conditions of the water sampling.

For description of the flow regime, seasonal coefficients of variations of the discharge (CV_Q) were computed in accordance to *Botter et al*. [2013]. Differences between the lc-excess of the water samples taken from the peatland drainage network, stream, and riparian zone were tested with the Kruskal-Wallis rank sum test (kruskal.test in R) followed by a post-hoc test after Nemenyi (posthoc.kruskal.nemenyi.test in R). We tested the data for normality with the Shapiro-Wilk test. We applied the Spearman rank-order correlation (coefficient give as ρ) to test relationships that are not normally distributed (e.g., monthly *Q*, monthly *P*, monthly *PET*, soil water lc-excess, distance to stream and altitude of sampling locations of the water samples in the extended peatland drainage network). For data that was normally distributed, we applied the Pearson correlation (e.g., average lc-excess and SD of lc-excess in the extended peatland drainage network, *Q* and PET_{14days} for the days of sampling in the extended drainage network (correlation coefficient given as r). The significance level was defined to be 0.05 for all statistical tests including. When we defined meteorological seasons, we refer to spring (April, March, May), summer (June, July, August), autumn (September, October, November), and winter (December, January, February).

4. Results

4.1. Hydroclimatic Dynamics

As for most years in the BB, precipitation (*P*) was quite evenly distributed throughout the study period (2/3 of all days were rainy days) with no strong seasonality (Figure 2a). Annual *P* ranged between 930 (2015) and 1200 mm yr^{-1} (2014). Median monthly *P* ($\pm$ standard deviation (SD)) was 78 mm/month ($\pm$53). Precipitation occurred mainly at low intensities, with 90% of the rainy days having $<$10 mm d^{-1} (summing up to 50% of the total precipitation amount) and 1/3 of the rainy days with less than 2 mm d^{-1} of *P*.

Annual potential evapotranspiration (*PET*) ranged between 460 (in 2012) and 520 mm yr^{-1} (in 2013). *PET* showed a strong seasonal variation with average *PET* rates of 2.3 to 2.7 mm d^{-1} from May to August and 0.3 to 0.7 mm d^{-1} from November to February (Figure 2b). However, maximum *PET* rates were between 3.5 and 6.5 mm d^{-1} from May to August.

Annual discharge (*Q*) varied between 440 (in 2015) and 900 mm yr^{-1} (in 2014, Figure 2e). Monthly sums of *Q* were positively correlated with monthly *P* ($\rho = 0.54$, $p < 0.001$) and negatively correlated with *PET* ($\rho = -0.57$, $p < 0.001$). On 90% and 40% of the days, *Q* was below 4 and 1 mm d^{-1}, respectively. However, during *P* events, the BB responded quickly and flow rates increased within few hours. *Q* was on average higher between November and February with mean values between 2.2 and 3.3 mm d^{-1}. From March to October, the average *Q* was between 1.7 and 0.8 mm d^{-1}. With minimum *Q* that usually did not drop below 1 mm d^{-1}, stream flows remained higher during winter than the base flow rates from spring to autumn. Hence, the flow regime, as defined by *Botter et al*. [2013], was more erratic during summer ($CV_Q = 1.31$) and autumn ($CV_Q = 1.37$), while more persistent and indifferent during winter ($CV_Q = 0.91$) and spring ($CV_Q = 1.05$), respectively. The variation of the seasonal CV_Q was positively correlated to mean seasonal *P* ($\rho = 0.52$, $p = 0.027$) and not correlated to the mean seasonal *PET* ($\rho = 0.24$, $p = 0.34$).

4.2. Stable Isotope Dynamics

The isotopic signal of *P* generally followed the seasonal variation of air temperature (*T*), with monthly lc-excess values being negatively correlated with *T* ($\rho = -0.63$, $p < 0.001$). The correlation of *P* lc-excess to *PET* was weaker ($\rho = -0.55$, $p < 0.001$). The lc-excess varied throughout the year, with lower monthly weighted average values (ranging between $-2.7‰$ and $-1.4‰$) between May and September and higher values ($+0.9‰$ to $+2.7‰$) between November and February (Figure 2a). However, the long term median of *P* lc-excess was $0.5‰$ (Table 1, supporting information Figure S1). The local meteoric water line (LMWL; $\delta^2H = 7.7 \times \delta^{18}O + 5.1$) was close to the GMWL.

The lc-excess signal of the BB stream water followed the seasonal variation of the *P* input, but its variation was only one-third of the variation in the *P* lc-excess (see SD in Table 1). However, the stream water lc-excess showed a lower correlation with *PET* ($\rho = -0.48$, $p = 0.001$) than *P* lc-excess ($\rho = 0.60$, $p < 0.001$). The lc-excess at the BB outlet was on average more depleted in heavy isotopes than the *P* input and most of the time greater than 0 (Table 1, Figure 2a, supporting information Figure S1). The regression between

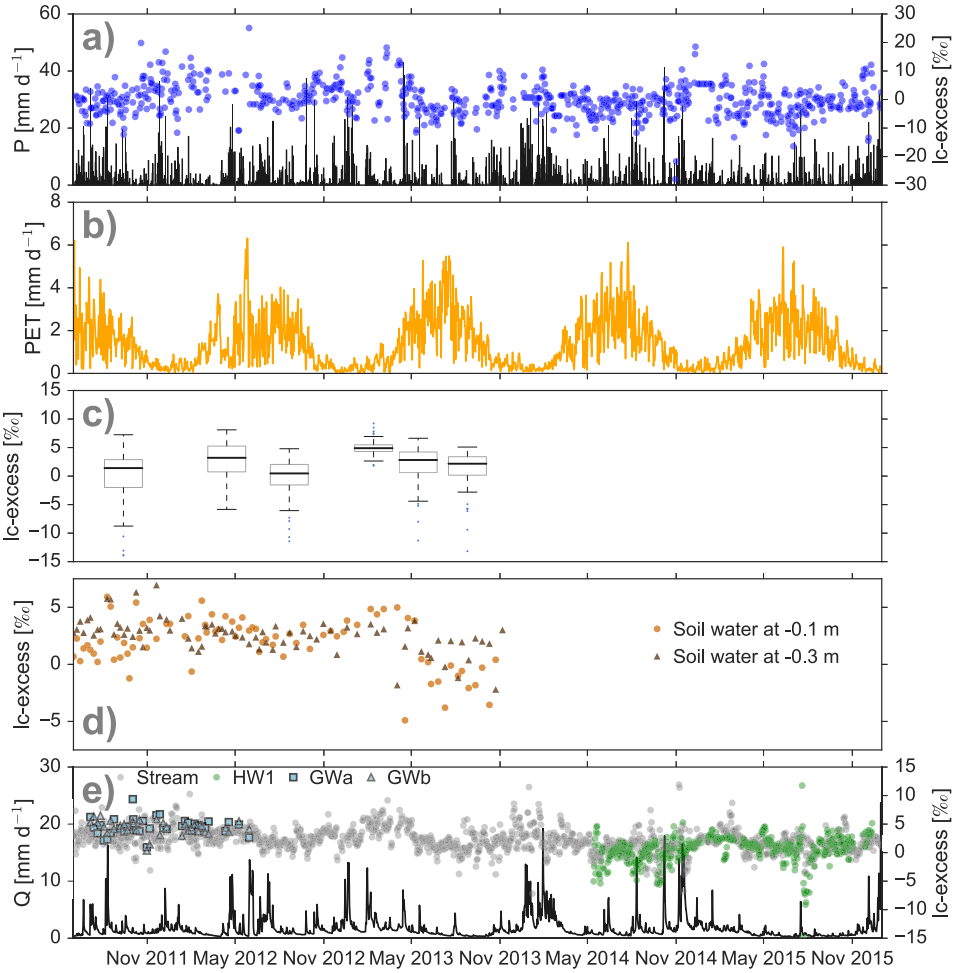

Figure 2. (a) Precipitation amount and isotopic signal as lc-excess; (b) potential evapotranspiration; (c) lc-excess of spatially distributed water samples in the valley bottom; (d) the isotopic signal as lc-excess of the water extracted from a peaty soil at 0.1 and 0.3 m depth; (e) discharge amount at the catchment outlet and the isotopic signal as lc-excess at the catchment outlet (Stream), at the subcatchment (HW1), and two groundwater wells (GWa and GWb).

$\delta^{18}O$ and $\delta^{2}H$ (the evaporation water line, EWL) had with 5.3‰ and −12.5‰ a lower slope and intercept than the LMWL.

The lc-excess of the mobile soil water sampled with the Rhizon samplers at −10 cm of the peat soil followed the *P* input signal (Figure 2d) and was correlated to the $lc\text{-}excess_{P14}$ ($\rho = 0.45$, $p < 0.001$). However, the variation of the lc-excess in the topsoil was damped compared to *P* by about 60% (Table 1). The mobile soil water was isotopically enriched from June to September with average monthly lc-excess values ranging between +1.4‰ and +1.8‰ and more depleted values (monthly averaged lc-excess >+3.1) from

Table 1. Median ± Standard Deviation of the lc-excess (‰) of the Precipitation Samples, Soil Water Samples Extracted Fortnightly With a Suction Cup Lysimeter, Stream Water at the BB Outlet, and Two Groundwater Wells Between 1 June 2011 and 6 November 2013 (n = Sample Numbers)[a]

Water Samples	Annual	n	Summer	Fall	Winter	Spring
Rainfall	0.5 ± 5.6	379	−3.5 ± 3.2	2.1 ± 4.3	1.5 ± 5.8	2.9 ± 7.3
SW 10	2.3 ± 2.2	81	1.5 ± 2.0	2.2 ± 2.0	3.8 ± 1.5	3.5 ± 2.3
SW 30	3.1 ± 1.4	80	2.9 ± 1.5	3.2 ± 1.7	3.2 ± 1	3.1 ± 1.3
Stream	2.7 ± 1.8	786	1.1 ± 1.4	2.7 ± 1.7	3.4 ± 1.7	3.9 ± 2.5
Groundwater a	4.5 ± 1.5	35	3.9 ± 1.5	4.4 ± 2.1	4.6 ± 0.5	4.9 ± 1.2
Groundwater b	4.5 ± 1.3	34	5.2 ± 1.0	4.7 ± 1.8	4.5 ± 0.7	4.1 ± 0.8

[a]The annual median isotope data are also shown in supporting information Figure S1.

November to March. The correlation of the monthly averages of the topsoil water lc-excess with *PET* had a Spearman's rank correlation coefficient of $\rho = -0.58$ ($p < 0.001$), which was stronger than for the precipitation or the stream water. The soil water isotopic signal at −30 cm was more damped than at −10 cm, since the standard deviation (SD) was only 20% of the SD of the *P* lc-excess (Table 1). The correlation between the monthly average lc-excess at −30 cm and the monthly average *PET* was relatively low ($\rho = -0.37$, $p = 0.04$) and no influence of the $lc\text{-}excess_{P14}$ was detected ($\rho = 0.09$, $p = 0.53$). Generally, the soil water samples had mostly an lc-excess >0 (above or on the LMWL), but dropped below 0 during the summer 2013 (Figure 2d). The EWL was for the mobile soil water with 5.3‰ and −12.4‰ for slope and intercept, respectively, very similar to the stream water EWL. The lc-excess of the mobile soil water in the peat soil generally followed the stream water signal at −10 cm ($\rho = 0.44$, $p < 0.001$) and −30 cm ($\rho = 0.32$, $p < 0.001$).

The groundwater had the most depleted isotope signals with an average lc-excess of +4.5‰ and generally very little variation throughout the year (Table 1 and Figure 2e). In contrast to the precipitation, stream, and mobile soil water, the groundwater lc-excess showed no correlation with the monthly mean *T* (for GWa: $\rho = -0.28$, $p = 0.40$; for GWb: $\rho = 0.43$, $p = 0.19$). All the groundwater samples plotted above the LMWL in a dual-isotope plot (lc-excess > 0) and the slope and intercept of the EWL were 4.2‰ and −22.4‰, respectively.

4.3. Spatiotemporal Dynamics of Evaporation Fractionation

The spatially distributed sampling of surface waters from water tracks and pools in the valley bottom of the BB showed that the water in the peatland drainage network deviated considerably from the LMWL, while the water from the riparian zone and the BB stream stayed usually above and generally close to the LMWL (Figure 3). The slope of the EWL for the peatland drainage network samples ranged accordingly between 3.9 (in September 2011) and 5.4 (in February 2013) (Table 2). The lower slopes of the EWLs show that the isotopic enrichment in the peatland drainage network was most pronounced for the sampling campaigns between May and September, while the winter samples followed the LMWL, indicating no or little evaporation fractionation (Figure 3a). The stream water and riparian zone in BB followed the temporal variation of the *P* input with more enriched isotopic signals during summer and depleted values during winter (Figures 3b and 3c). The water samples of the riparian zone did not differ significantly from the stream water samples in terms of their median lc-excess values at any sampling date (indicated with lower case letters in Figure 4a). In contrast, the lc-excess of the peatland drainage network was significantly different from the water in the stream and riparian zone for half of the sampling campaigns (September 2011, April 2012, and May 2013). For the peatland drainage network, the variation of the lc-excess was lowest in February 2013, where a significantly different lc-excess was found compared to the other sampling campaigns (indicated by upper case letters in Figure 4b). The spring (in April 2012 and May 2013) and summer/fall sampling (in September 2011, August 2012) of the peatland drainage network formed two different groups that differed significantly from each other in terms of their lc-excess (Figure 4b).

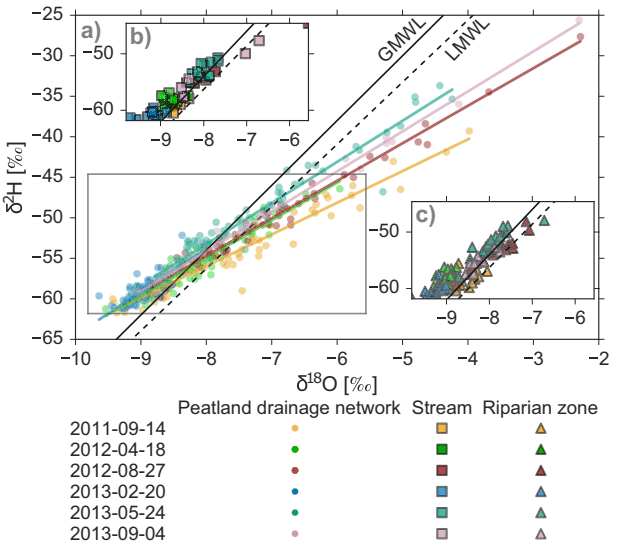

Figure 3. Dual-isotope plot of the spatially distributed sampling of the water in (a) the peatland drainage network, (b) the stream, and (c) the riparian zone. All samples were taken in parallel on six different days. See statistic of the regression lines (evaporation water lines) in Table 2.

There was a pronounced spatial variability in the lc-excess pattern in the peatland drainage network. The average lc-excess was lower (indicating higher evaporation fractionation) in the center of the bog-fen complexes (green open symbols in Figure 5a). Toward the edges, the lc-excess

Table 2. Overview of the Spatially Distributed Saturated Area and Stream Sampling Campaigns: The Average lc-excess (± Standard Deviation) of the Saturated Area Samples and Stream Water Samples; n = Sample Numbers, Q = Discharge at the Outlet on the Sampling Day, PET = Potential Evapotranspiration on the Sampling Day, PET_{14} = Average Potential Evapotranspiration on the 14 Days Prior to the Sampling Day, P = Precipitation on the Sampling Day, P_{14} = Precipitation Sum Over the 14 Days Prior to the Sampling Date, Slope, and Intercept to Characterize the Regression for the Samples of the Saturated Area in a Dual Isotope Plot, and Spearman Rank Correlation ρ of the $\delta^{18}O$ to $\delta^{2}H$ Relation of the Particular Saturated Area Sampling Campaign (All Significant at $p < 0.01$)

Date	Sat. Area lc-excess (‰)	n	Stream lc-excess (‰)	Q (mm d^{-1})	PET (mm d^{-1})	PET_{14} (mm d^{-1})	P (mm d^{-1})	P_{14} (mm 14 d^{-1})	Slope	Intercept (‰)	Spearman Rank corr. ρ
14 Sep 2011	0.28 ± 4.37	94	2.69 ± 0.90	0.97	1.8	1.5	1.1	46	3.90	−24.50	0.96
18 Apr 2012	3.17 ± 2.66	94	4.49 ± 1.39	1.76	0.7	1.0	3.6	36	4.71	−17.33	0.94
27 Aug 2012	0.08 ± 3.61	83	1.52 ± 3.45	1.13	0.7	1.7	13.7	48	4.65	−17.56	0.98
20 Feb 2013	5.20 ± 1.18	92	5.30 ± 1.41	2.75	0.5	0.7	1.9	21	5.36	−10.88	0.80
24 May 2013	2.39 ± 3.00	94	3.66 ± 1.15	1.59	2.6	1.8	1.6	41	5.06	−12.70	0.96
4 Sep 2013	1.03 ± 4.09	35	2.09 ± 2.24	0.33	2.5	2.6	0.0	7	4.93	−14.69	0.99

increased, which indicates increasing groundwater influence. In fact, as more the sampling location was located within the area covered by peat soil (dark brown in Figure 1), the higher was the evaporation signal ($\rho = -0.70$, $p < 0.01$). Toward the minerogenic soils, the groundwater seepage into the peatland drainage network increases. The sample locations outside the peat soil cover had an almost constant average lc-excess signal (range between +2‰ and +4‰) and did not show a dependency on the distance to the peat soils ($\rho = -0.18$, $p = 0.40$). Both altitude and distance to the stream of the sampling locations showed a significant relation to the average lc-excess of the individual sampling locations, but they were relatively weak

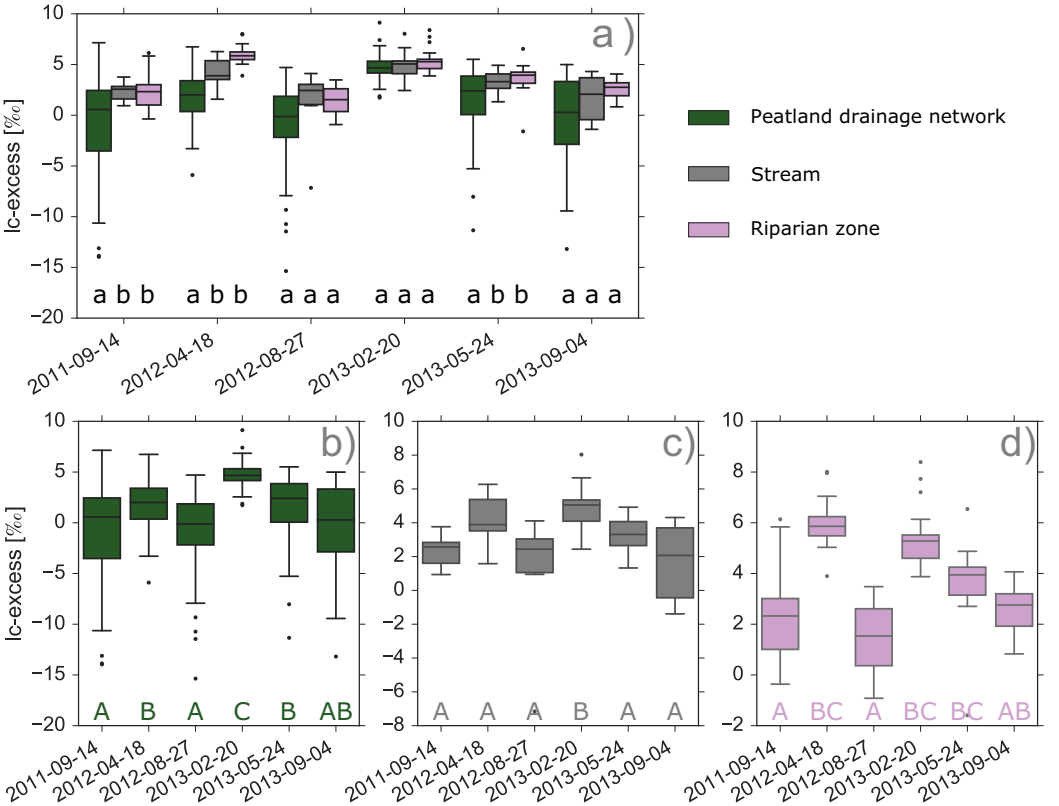

Figure 4. Variation of lc-excess for the six different sampling campaigns in the three landscape units (peatland drainage network = green, stream = grey, and riparian zone = purple). Note that the *x* axis is not a date axis, but represents the sampling date classes. (a) Variation between the landscape units on each sampling day. Lowercase letters at the date indicate significant differences between the landscape units for that day. This means, the data of the boxplots with the same lower case letter for the particular sampling day do not differ significantly. (b)–(d) Variation within one landscape unit between different sampling days. Different capital letters indicate significant differences between the sampling times within each landscape unit. This means, the data of the boxplots in each subplot that have the same capital letter do not differ significantly.

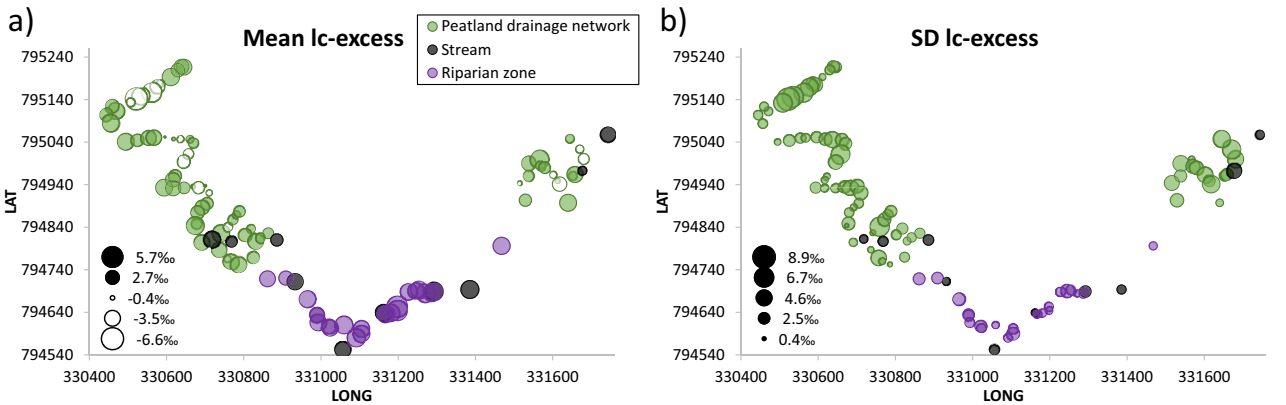

Figure 5. Spatial distribution of (a) the mean lc-excess and (b) the standard deviation (SD) of the lc-excess over the six water sampling campaigns in the peatland drainage network (green), the main stream (grey), and the riparian zone (purple). In Figure 5a, filled symbols indicate positive lc-excess and open symbols indicate negative lc-excess, while the size of the symbols shows the deviation from lc-excess = 0. In Figure 5b, the size of the symbol represents the standard deviation of the lc-excess at the sampling point over the six sampling campaigns. Measured values for each sampling point and campaign are shown in supporting information Figure S2.

predictors of the lc-excess pattern ($\rho = -0.23$ and $\rho = -0.36$, respectively). Thus, we conclude that in our environment the pedogenic landscape characteristics are more important than topographic conditions.

The variability of the lc-excess in space, given as the SD over all six sampling campaigns, was highly correlated with the mean lc-excess ($\rho = -0.76$, $p < 0.01$). Consequently, the spatial pattern of the SD of lc-excess was more marked toward the center of the riparian drainage network, but relatively low at the edge of the bog-fen complex, in the stream and the riparian zone (Figure 5b). Thus, the missing temporal variability toward the edge of the bog-fen complex is consistent with groundwater seepage from minerogenic soils into the peatland drainage network.

The mean lc-excess of the water samples from the peatland drainage network showed a strong negative correlation with PET_{14days} (Figure 6a), while the variation of lc-excess was positively related to PET_{14days} (Figure 6c). For comparison, also the soil water lc-excess at −10 cm soil depth correlated with PET_{14days} ($\rho = -0.41$, $p < 0.01$). However, the lc-excess at −30 cm soil depth ($\rho = -0.19$, $p = 10$) and the groundwater lc-excess (GWa: $\rho = -0.18$, $p = 0.3$; GWb: $\rho = 0.33$, $p = 0.05$) both showed no strong relationship with PET_{14days}. The mean lc-excess from the peatland drainage network further correlated significantly with discharge on the sampling day (Figure 6b) and the spatial variability was significantly negatively correlated with discharge (Figure 6d). Given these findings of the spatiotemporal patterns of the lc-excess within the bog-fen complex (Figures 5 and 6), evaporation fractionation mostly seems to take place within the saturated area of the raised bog during dry periods of high radiative forcing. Meanwhile, the groundwater influence at the edge of the peatland drainage network keeps the lc-excess values high in the fen, leading to high variabilities within the bog-fen complex. With higher precipitation input of nonfractionated water and a better hydraulic connectivity within the peatland drainage network, the fractionation signal gets lower and approaches the groundwater signal. If evaporation increases again, the water of the bog-fen complex will increasingly evaporate on their way through the peatland drainage network, leading to an isotopic enrichment and lower lc-excess with higher *PET* rates.

4.4. Effects of Evaporation Fractionation on the Variability of Stream Water Isotope Signature

During most of the year, there is a linear relation between the isotopic composition at the HW1 outlet and the BB outlet. In summer, the discharge at the outlet of HW1 is enriched in heavy isotopes compared to the water at the BB outlet (Figures 7a and 7b). The linear relationship during most of the year indicates that the offset during summer is not caused by faster routing or lower groundwater contribution in the HW1 than in BB. Instead, the evaporation fractionation signal in the peatland drainage network is consistent with the offset between HW1 and the stream in BB. The lc-excess data support the influence of kinetic fractionation, since the lc-excess was more negative during summer for the outflow at HW1 than for the BB outlet (Figure 7c). This difference in lc-excess is correlated with Q for the low flows ($Q < 0.75$ mm d^{-1}, exceeded in 70% of the time) with HW1 being more isotopically enriched than BB for lower flows ($\rho = -0.32$, $p < 0.001$).

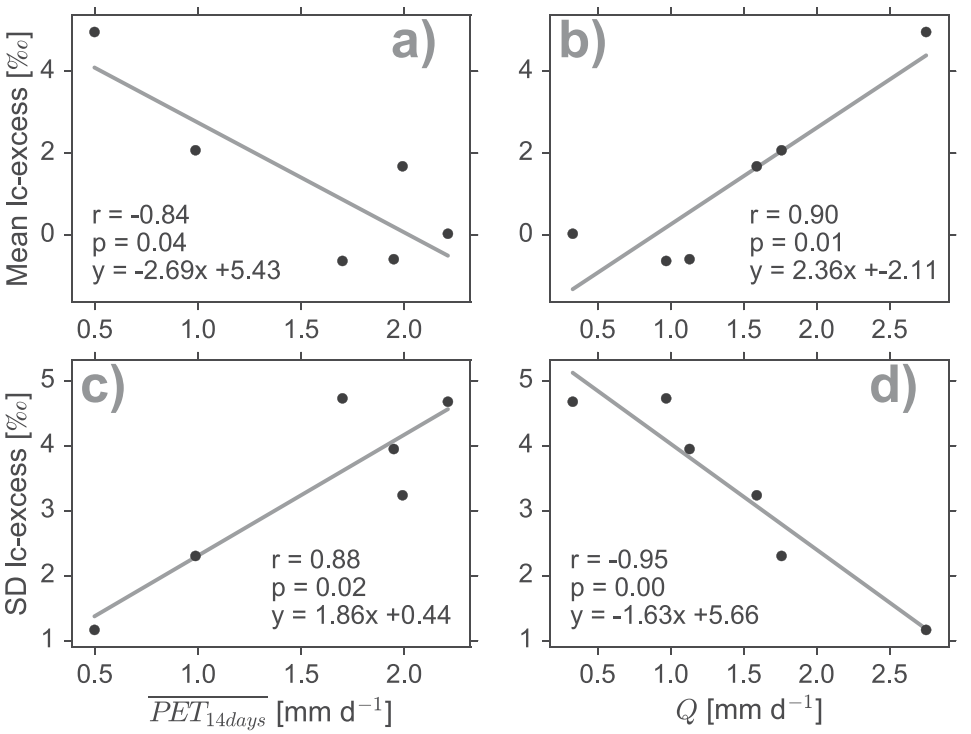

Figure 6. Mean value and standard deviation of the lc-excess of the spatially distributed sampling of the water of the peatland drainage network and its relation to (a and c) the 14 days' average potential evapotranspiration prior to the sampling and (b and d) the discharge on the day of sampling, respectively.

5. Discussion

5.1. The lc-excess Dynamics in Stream, Soil, and Groundwater as a Result From an Interplay of P and PET

The long term daily input-output isotope data from the BB revealed that in such wet temperate/boreal climate, the seasonal variability of the lc-excess in the precipitation is imprinted on the stream water. The stream water lc-excess was mostly depleted in heavy isotopes compared to the average signal of the precipitation due to the influence of the isotopically depleted groundwater contribution to the discharge. However, the influence of *PET* on the stream water lc-excess is seen in the lower slope of the EWL for the stream compared to *P*. Hence, water was not simply routed through the system, but its ratio between ^{18}O and ^{2}H was affected due to kinetic fractionation.

Further, the persistence of the high lc-excess in the groundwater indicated that the seasonal dynamics of the *PET* led to preferential evapotranspirative water losses: Isotopically enriched summer rain was more likely to be recycled back into the atmosphere via transpiration and evaporation, than isotopically depleted winter rain. This time variant partitioning of *P* into *ET* and *Q* affects the isotopic composition due to seasonal changes in the mass balance, which act independently from isotopic fractionation processes. As a result, the isotopically depleted winter precipitation was more likely to recharge the groundwater storage or to be routed to the stream network than the summer rain. Since 80–95% of the BB discharge is usually pre-event water [*Tetzlaff et al*., 2014], namely a mixture of groundwater and overland flow from the saturated valley bottom [*Soulsby et al*., 2015], the continuous supply of the isotopically depleted groundwater has an influence on the stream water lc-excess. A more depleted signal in the groundwater, reflecting that groundwater recharge is dominated by winter precipitation, was shown in several isotope studies [e.g., *O'Driscoll et al*., 2005; *Yeh et al*., 2011; *Bertrand et al*., 2012].

Similar to the stream water, the lc-excess of mobile soil water in the peat soil also reflected the interplay of *P* and *ET* forcing. While the significant contribution of isotopically depleted groundwater damped the stream water lc-excess, the mobile soil water lc-excess was damped by the generally high water storage capacity in the peat soil. Since the volumetric water content seldom drops below 80% [*Tetzlaff et al*., 2014],

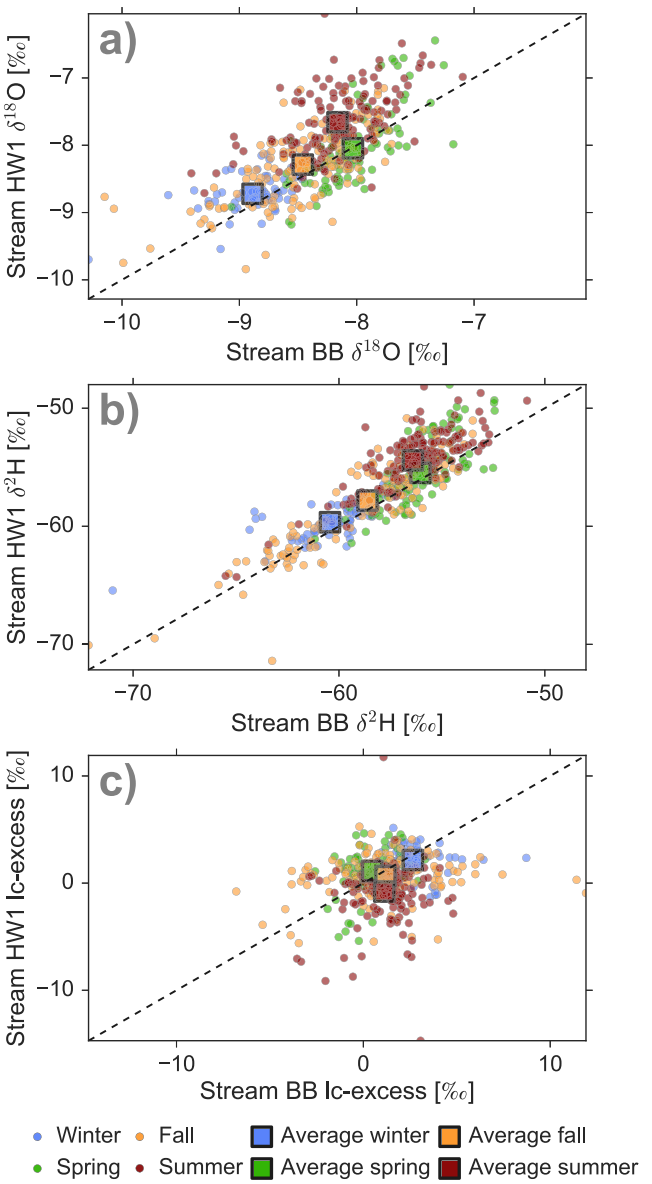

Figure 7. Comparison between water in the outflow of the subcatchment HW1 (Stream HW1) and the Bruntland Burn catchment outlet (Stream BB) and its δ^{18}O, δ^{2}H, and lc-excess composition. Daily sampling took place in parallel between June 2014 and December 2015. Points indicate daily values and squares represent seasonal averages.

infiltrating rain water will usually rapidly mix with a higher pre-event water volume in the soil. Similar to the preferential groundwater recharge with isotopically depleted water, also the soil water volume will get depleted in heavy isotopes compared to annual *P*, since the isotopic enriched summer rains will be preferentially evaporated. The low variability of the soil water lc-excess at −30 cm and the lack of a correlation with *P* lc-excess and PET_{14days}, supports earlier findings based on hydrometric and deuterium analysis by *Tetzlaff et al.* [2014], who concluded that the seepage from the peat soils into the BB is relatively well mixed. Generally, the peat soils seem to be well connected to the stream, since their lc-excess values correlate with each other. Thus, our findings corroborate earlier findings that the lateral flow in the upper soil horizon of peat soils maintain the connectivity between the landscape and stream [e.g., *Tetzlaff et al.*, 2007].

The influence of evaporation on the soil water isotopic signal is shown in the slope of the EWL. However, since the mobile water samples generally plot close to the LMWL the impact of evaporation fractionation is low and generally limited to the topsoil. Our mobile soil water isotope data are thus in line with other studies that did not report evaporation fractionation of soil waters when sampled with suction cup lysimeters [*Brooks et al.*, 2010] or wick samplers [*Timbe et al.*, 2014]. In contrast, sampling of the bulk soil water in Mediterranean and arid climates showed a much higher fractionation signal, as reviewed by *Sprenger et al.* [2016a]. However, bulk soil water sampling with cryogenic extraction or centrifugation in the BB showed only limited evidence of fractionation at −10 and −30 cm soil depth [*Geris et al.*, 2015].

5.2. Extended Peatland Drainage Networks as Hot Spots of Evaporation Fractionation

In contrast to the stream and mobile soil water, the interconnected water pools of the peatland drainage network clearly serve as hot spots of evaporation fractionation, since water samples collected from there plot below the LMWL when *PET* is high. The interplay between *P* input, evaporative losses, and wetness is conceptualized in Figure 8. During wet conditions ("rainfall driven" case), when *Q* and the saturation area extent are high, the peatland drainage network is well connected. Due to low *PET* and water input of unfractionated *P*, the lc-excess is generally high (>1‰) and the variation in lc-excess within the peatland drainage network is low. Water is routed quickly through the catchment, leading to low water ages of the saturation

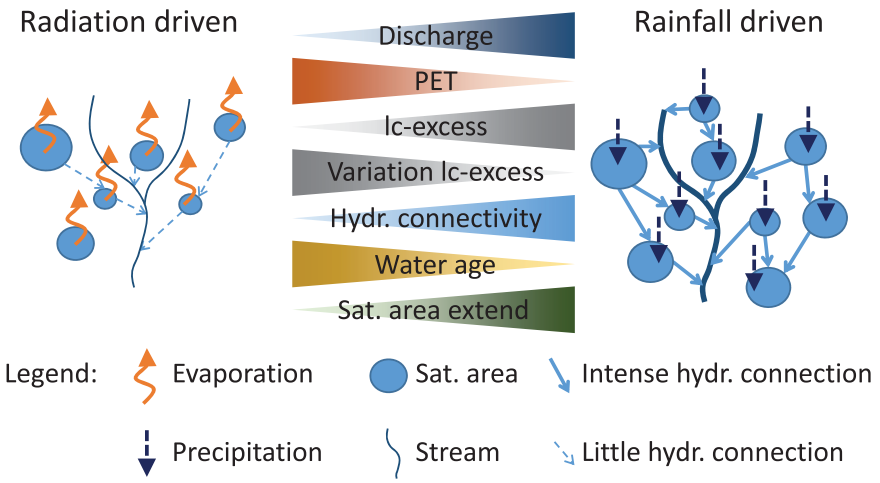

Figure 8. Conceptual graphic visualizing the dominant drivers that lead to the observed temporal variability of the evaporation fractionation signal in the peatland drainage network that influences the stream water isotopic composition.

overland flow as described by *Soulsby et al*. [2015]. With decreasing *Q*, the lc-excess within the peatland drainage network decreases. With increasing *PET* and less rainfall input ("radiation driven" case), evaporation fractionation will be enhanced and lead to lower lc-excess in the water pools and tracks of the peatland drainage network. Water travel times will increase during these dry periods, and depending on the differences of the pools in their size, exposure to radiation, and connectivity to other the pools or the drainage system the lc-excess variability within the peatland drainage network will increase. At this catchment state, the peatland drainage system experiences intense evaporation losses, which is reflected in the EWL of the water samples.

The slopes of the EWL for the water samples of the peatland drainage network are in the range of simulations for lakes of the northern latitudes [*Gibson et al*., 2008]. However, our results also showed that the EWL are time-variant with lower slopes and intercepts during high *PET* and higher slope and intercept during low *PET*. These findings are therefore in contrast to the "single well-defined local evaporation lines" as suggested by *Gibson et al*. [1993]. The variability of the slope of the EWL is driven by the seasonally variable evaporation. The seasonally variable isotopic composition of *P* influences from which point on the LMWL the water samples deviate along the EWL. This intersection of the LMWL and EWL will move in the dual-isotope space toward enriched isotopic values for the summer period and toward depleted isotopic values for the winter period.

Similar to our results, a pronounced seasonal difference in the lc-excess of water pools in peatland drainage network was found by *Carrer et al*. [2016]. Their sampling in October plotted close to the LMWL, while the sampling in June showed a high variation along a EWL depending on the water residence times within the peatland drainage network. Therefore, our finding that the dynamic balance between the nonfractionated precipitation signal and fractionating evaporation signal in the peatland drainage network are depended on the catchment wetness is in line with *Carrer et al*. [2016].

5.3. Fractionation Signal of Peatland Passed on to the Stream

When the peatland drainage network experiences intense evaporation (Figure 8), the fractionated water will eventually drain into the main stream channel. Therefore, we see an isotopically enriched signal for the outlet of HW1, whose valley bottom consist of a greater coverage of ombrogenous peatland, compared to the outlet of BB, whose valley bottom consists of a mixture of peaty gleys and peat soils receiving minerogenic drainage. Our findings based on lc-excess corroborate the results from a multitracer approach, showing that the groundwater contribution to the stream increases downstream of HW1 [*Blumstock et al*., 2015]. *Blumstock et al*. [2015] further revealed that HW1 showed more evaporation fractionation than adjacent headwater catchments with much lower peat soil coverage. The presence of the peatland and the lower influence of isotopically depleted groundwater in HW1 characterize the main difference to the BB. The extended saturated area with water pools and drainage tracks exposed to the atmosphere allows

evaporation to occur. Therefore, an evaporation fractionation signal in stream water is not limited to catchments where lakes are present [e.g., *Burns and McDonnell*, 1998] or under climates with intensive *ET* [*Klaus et al*., 2015], but can also occur under relatively low *ET* when surface drainage networks include open water pools and tracks, such as those that develop in peatland drainage network receiving shallow soil water as in the case of the BB.

Gibson and Reid [2010] found a weak correlation between stream water $\delta^{18}O$ and *Q* during the summer for a catchment covered with 21% surface water (349 perennial lakes) [*Spence*, 2006] and 15% peatland and related these to evaporation enrichment. Our results are generally in line with their findings even though in our case the surface water extent is much lower and not represented by lakes. By using a dual-isotope approach with the lc-excess, the influence of the variation from the precipitation input is lowered. A limitation of the analysis to either $\delta^{18}O$ or $\delta^{2}H$ would not be able to rule out the isotopic variability in the precipitation input to cause the variability in the extended peatland drainage network and stream water. Only by considering the relationship of the two isotopes, the nonequilibrium processes due to evaporation can be revealed. However, as with *Gibson and Reid* [2010], the relation between *Q* and the evaporation fractionation signal in the stream water is relatively low, indicating variation in *ET* has a stronger influence than *Q*. Nevertheless, the fact that the differences between the lc-excess of HW1 and BB diminishes with elevated discharge indicates that overland flow is rapidly generated, as usually found in catchments with peatlands [*Laudon et al*., 2007]. This way, the water pools in the peatland rapidly reconnect and the precipitation signal is translated to the stream water isotope composition. The described processes—how the evaporation fractionation signal induced by the saturated soils of the peatland influences the stream water isotopic composition—are in contrast to the findings for unsaturated soils (vadose zone). Water infiltrating into the vadose zone also experiences evaporation fractionation in the upper soil, but the soil water is not hydrologically connected to the drainage system under these conditions and will, therefore, not translate the fractionation signal to the stream (or groundwater). Instead, the soil water of the topsoil, that experienced evaporation fractionation, is relative to the entire subsurface water of low mass. Thus, when the subsurface flow is activated due to rainfall input, the evaporation signal will reduce or disappear by the percolation and dispersion in the recharge process [*Sprenger et al*., 2016a].

5.4. Wider Implications

The evaporation fractionation in the peatland drainage network presented in this study and the resulting difference in the outflow of the nested catchments question the often made assumption that the stream water draining catchments does not show evidence of isotopic fractionation processes. Thus, it appears to be relevant to account for the isotopic enrichment due to evaporation losses at surface waters that are connected to the stream network. While this is obvious for lakes and ponds, our study shows that also saturated areas, where drainage waters experience long residence times and are exposed to radiation forcing show an evaporation fractionation signal. This has implications for tracer aided runoff modeling and the estimation of travel times [*Birkel and Soulsby*, 2015].

Not including this enriched isotopic signal in the drainage network may bias the model parameters if isotope data are part of the objective function for model calibration: For a model that assumes that no evaporation fractionation is taking place, the flow velocities could be overestimated to route the enriched summer precipitation signal through the system in order to fit the simulation to the observations. This way, travel times may be underestimated. A similar bias would also affect hydrograph separation techniques. Further, the information about the mechanisms of evaporation enrichment in different landscape unites within a catchment can help to better understand the spatial variability of the amount and intensities of evaporation losses. Also the partitioning between the fractionating evaporation and nonfractionating transpiration, which is relevant for isotope mass balance analysis [*Smith et al*., 2016] can be constrained by the assessment of the water stable isotope variability across the catchment. The combined knowledge of the saturated area extend [*Birkel et al*., 2010] and the isotopic fractionation within this area would facilitate evaporation estimates for these parts of a catchment using the Craig-Gordon model [see *Horita et al*., 2008]. However, such a spatially resolved estimation of evaporation losses would require microclimatic data representing individual pools and tracks within the drainage network, to adequately parameterize the Craig-Gordon model for local conditions. Standard weather data would not be sufficiently sensitive to account for the local variability. Incorporating such spatial information of evaporation losses and isotopic enrichment in an isotope mass balance would then limit the range of potential contributions from flow paths of the

unsaturated zone, which usually do not show a fractionation signal (Figure 2d). The data presented on spatially distributed stable isotope concentrations across a peatland drainage network could further be used to quantitatively assess the mixing between surface water and groundwater, which would go beyond the scope of the current study. Such modeling focus on the here presented data set will be focus of future work.

6. Conclusion

Our study used the lc-excess within different compartments of two nested headwater catchments as a signal of evaporation fractionation of water stable isotopes, and has shown the potentially high impact of peatland drainage networks on the stream water isotopic composition. The interplay of unfractionated rainfall input, evaporation losses inducing kinetic fractionation, hydraulic connectivity, and groundwater influence in a bog-fen complex, alters the isotopic signal in the catchment outflow in a time variable manner. During dry periods, when the discharge rates are low and the potential evapotranspiration is high, the water in the peatland drainage network becomes isotopically enriched. These findings are in contrast to the isotope data from other headwater catchments where no peatland is present and stream water plots along the LMWL. The fractionation processes in peatland drainage networks and the accompanying alteration of the stream water isotopic signal at the catchment outlet have implications for tracer-aided hydrological modeling. The common assumption that stream water does not experience kinetic fractionation does not always hold under conditions such as those presented. Hence, models need to consider the effect of extended peatland drainage networks in the simulation of the water stable isotope routing through the hydrologic system. The findings are likely to apply, but may not be limited, to similar headwater catchments with extended peatlands which cover large areas in the northern latitudes. Also wetlands in other parts of the world could have a similar effect on the stream water isotopic composition. Our study underlined not only the importance of peatland drainage networks for controlling the processes of subsurface mixing, but included as well their distinguished role for evaporation losses.

The dual-isotope approach in our study using the lc-excess showed advantages over simpler and direct analysis of δ^2H or δ^{18}O to better distinguish between the influences of the variation of the isotopic signal in the rainfall input and the isotopic enrichment due to evaporation fractionation on the stream water isotope data. The nested catchment approach and the spatially distributed sampling within the catchments further provided a unique insight into the variability of the fractionation signal across different landscape units. Such information will be valuable to constrain and benchmark hydrological models for getting a better representation of the hydrological processes within a catchment that lead to the signal measured at the catchment outlet.

Acknowledgments
We would like to thank the European Research Council (ERC, project GA 335910 VeWa) and Natural Environment Research Council NERC (project NE/K000268/1) for funding. We also want to thank Christian Birkel for the initial spatial distributed surveys of the tracers. The data are available from the corresponding author upon request. We thank the Associate editor and three anonymous reviewers for their feedback during the peer-review process.

References

Allison, G. B., C. Barnes, C. M. Hughes, and F. Leaney (1984), Effect of climate and vegetation on oxygen-18 and deuterium profiles in soils, in *Isotope Hydrology 1983*, edited by IAEA, pp. 105–122, Int. At. Energy Agency, Vienna.

Anderton, S. P., J. Latron, S. M. White, P. Llorens, F. Gallart, C. Salvany, and P. E. O'Connell (2002), Internal evaluation of a physically-based distributed model using data from a Mediterranean mountain catchment, *Hydrol. Earth Syst. Sci.*, *6*(1), 67–84, doi:10.5194/hess-6-67-2002.

Bertrand, G., J. Masini, N. Goldscheider, J. Meeks, V. Lavastre, H. Celle-Jeanton, J.-M. Gobat, and D. Hunkeler (2012), Determination of spatio-temporal variability of tree water uptake using stable isotopes (δ^{18}O, δ^2H) in an alluvial system supplied by a high-altitude watershed, Pfyn forest, Switzerland, *Ecohydrology*, *7*(2), 319–333, doi:10.1002/eco.1347.

Birkel, C., and C. Soulsby (2015), Advancing tracer-aided rainfall-runoff modelling: A review of progress, problems and unrealised potential, *Hydrol. Processes*, *29*(25), 5227–5240, doi:10.1002/hyp.10594.

Birkel, C., D. Tetzlaff, S. M. Dunn, and C. Soulsby (2010), Towards a simple dynamic process conceptualization in rainfall-runoff models using multi-criteria calibration and tracers in temperate, upland catchments, *Hydrol. Processes*, *24*(3), 260–275, doi:10.1002/hyp.7478.

Birkel, C., D. Tetzlaff, S. M. Dunn, and C. Soulsby (2011), Using time domain and geographic source tracers to conceptualize streamflow generation processes in lumped rainfall-runoff models, *Water Resour. Res.*, *47*, W02515, doi:10.1029/2010WR009547.

Birkel, C., C. Soulsby, and D. Tetzlaff (2014), Developing a consistent process-based conceptualization of catchment functioning using measurements of internal state variables, *Water Resour. Res.*, *50*, 3481–3501, doi:10.1002/2013WR014925.

Blumstock, M., D. Tetzlaff, I. A. Malcolm, G. Nuetzmann, and C. Soulsby (2015), Baseflow dynamics: Multi-tracer surveys to assess variable groundwater contributions to montane streams under low flows, *J. Hydrol.*, *527*, 1021–1033, doi:10.1016/j.jhydrol.2015.05.019.

Blumstock, M., D. Tetzlaff, J. J. Dick, G. Nuetzmann, and C. Soulsby (2016), Spatial organisation of groundwater dynamics and streamflow response from different hydropedological units in a montane catchment, *Hydrol. Processes*, *30*, 3735–3753, doi:10.1002/hyp.10848.

Botter, G., E. Bertuzzo, and A. Rinaldo (2010), Transport in the hydrologic response: Travel time distributions, soil moisture dynamics, and the old water paradox, *Water Resour. Res.*, *46*, W03514, doi:10.1029/2009WR008371.

Botter, G., S. Basso, I. Rodriguez-Iturbe, and A. Rinaldo (2013), Resilience of river flow regimes, *Proc. Natl. Acad. Sci. U. S. A.*, *110*(32), 12,925–12,930, doi:10.1073/pnas.1311920110.

Brooks, J. R., H. R. Barnard, R. Coulombe, and J. J. McDonnell (2010), Ecohydrologic separation of water between trees and streams in a Mediterranean climate, *Nat. Geosci.*, *3*(2), 100–104, doi:10.1038/NGEO722.

Bullock, A., and M. Acreman (2003), The role of wetlands in the hydrological cycle, *Hydrol. Earth Syst. Sci.*, *7*(3), 358–389, doi:10.5194/hess-7-358-2003.

Burns, D. A., and J. J. McDonnell (1998), Effects of a beaver pond on runoff processes: Comparison of two headwater catchments, *J. Hydrol.*, *205*(3–4), 248–264, doi:10.1016/S0022-1694(98)00081-X.

Carrer, G. E., A. N. Rousseau, S. Jutras, and M. Fossey (2016), Assessment of the impact of pools on the water isotopic signature of a boreal patterned peatland, *Hydrol. Processes*, *30*(8), 1292–1307, doi:10.1002/hyp.10715.

Craig, H., and L. I. Gordon (1965), Deuterium and oxygen 18 variations in the ocean and the marine atmosphere, in *Stable Isotopes in Oceanographic Studies and Paleotemperatures*, edited by E. Tongiorgi, pp. 9–130, Lab. di Geol. Nucl., Pisa, Italy.

Craig, H., L. I. Gordon, and Y. Horibe (1963), Isotopic exchange effects in the evaporation of water: 1. Low-temperature experimental results, *J. Geophys. Res.*, *68*(17), 5079–5087, doi:10.1029/JZ068i017p05079.

Dansgaard, W. (1964), Stable isotopes in precipitation, *Tellus*, *16*(4), 436–468, doi:10.1111/j.2153-3490.1964.tb00181.x.

Dick, J. J., D. Tetzlaff, and C. Soulsby (2015), Landscape influence on small-scale water temperature variations in a moorland catchment, *Hydrol. Processes*, *29*(14), 3098–3111, doi:10.1002/hyp.10423.

Dunn, S. M., and R. Mackay (1995), Spatial variation in evapotranspiration and the influence of land use on catchment hydrology, *J. Hydrol.*, *171*(1–2), 49–73, doi:10.1016/0022-1694(95)02733-6.

Evaristo, J., S. Jasechko, and J. J. McDonnell (2015), Global separation of plant transpiration from groundwater and streamflow, *Nature*, *525*(7567), 91–94, doi:10.1038/nature14983.

Geris, J., D. Tetzlaff, J. McDonnell, J. Anderson, G. Paton, and C. Soulsby (2015), Ecohydrological separation in wet, low energy northern environments? A preliminary assessment using different soil water extraction techniques, *Hydrol. Processes*, *29*(25), 5139–5152, doi:10.1002/hyp.10603.

Gibson, J. J., and T. W. D. Edwards (2002), Regional water balance trends and evaporation-transpiration partitioning from a stable isotope survey of lakes in northern Canada, *Global Biogeochem. Cycles*, *16*(2), doi:10.1029/2001GB001839.

Gibson, J. J., and R. Reid (2010), Stable isotope fingerprint of open-water evaporation losses and effective drainage area fluctuations in a subarctic shield watershed, *J. Hydrol.*, *381*(1–2), 142–150, doi:10.1016/j.jhydrol.2009.11.036.

Gibson, J. J., T. W. Edwards, G. G. Bursey, and T. D. Prowse (1993), Estimating evaporation using stable isotopes: Quantitative results and sensitivity analysis for two catchments in northern Canada, *Hydrol. Res.*, *24*(2–3), 79–94.

Gibson, J. J., J. S. Price, R. Aravena, D. F. Fitzgerald, and D. Maloney (2000), Runoff generation in a hypermaritime bog-forest upland, *Hydrol. Processes*, *14*(15), 2711–2730, doi:10.1002/1099-1085(20001030)14:15<2711::AID-HYP88>3.0.CO;2-2.

Gibson, J. J., S. J. Birks, and T. W. D. Edwards (2008), Global prediction of δA and δ^2H-δ^{18}O evaporation slopes for lakes and soil water accounting for seasonality, *Global Biogeochem. Cycles*, *22*, GB2031, doi:10.1029/2007GB002997.

Gore, A. J. (1983), Introduction, in *Mires: Swamp, Bog, Fen, and Moor, Ecosystems of the World*, vol. 4A, edited by A. J. Gore, pp. 1–30, Elsevier, Amsterdam.

Harman, C. J. (2015), Time-variable transit time distributions and transport: Theory and application to storage-dependent transport of chloride in a watershed, *Water Resour. Res.*, *51*, 1–30, doi:10.1002/2014WR015707.

Horita, J., K. Rozanski, and S. Cohen (2008), Isotope effects in the evaporation of water: A status report of the Craig-Gordon model, *Isot. Environ. Health Stud.*, *44*(1), 23–49, doi:10.1080/10256010801887174.

Isokangas, E., K. Rozanski, P. M. Rossi, A.-K. Ronkanen, and B. Kløve (2015), Quantifying groundwater dependence of a sub-polar lake cluster in Finland using an isotope mass balance approach, *Hydrol. Earth Syst. Sci.*, *19*(3), 1247–1262, doi:10.5194/hess-19-1247-2015.

Klaus, J., J. J. McDonnell, C. R. Jackson, E. Du, and N. A. Griffiths (2015), Where does streamwater come from in low-relief forested watersheds? A dual-isotope approach, *Hydrol. Earth Syst. Sci.*, *19*(1), 125–135, doi:10.5194/hess-19-125-2015.

Landwehr, J. M., and T. B. Coplen (2006), Line-conditioned excess: A new method for characterizing stable hydrogen and oxygen isotope ratios in hydrologic systems, in *International Conference on Isotopes in Environmental Studies*, pp. 132–135, Int. At. Energy Agency, Vienna.

Laudon, H., V. Sjöblom, I. Buffam, J. Seibert, and M. Mörth (2007), The role of catchment scale and landscape characteristics for runoff generation of boreal streams, *J. Hydrol.*, *344*(3–4), 198–209, doi:10.1016/j.jhydrol.2007.07.010.

Lessels, J. S., D. Tetzlaff, C. Birkel, J. Dick, and C. Soulsby (2016), Water sources and mixing in riparian wetlands revealed by tracers and geospatial analysis, *Water Resour. Res.*, *52*, 456–470, doi:10.1002/2015WR017519.

McGuire, K. J., and J. J. McDonnell (2006), A review and evaluation of catchment transit time modeling, *J. Hydrol.*, *330*(3–4), 543–563, doi:10.1016/j.jhydrol.2006.04.020.

O'Driscoll, M., D. DeWalle, K. McGuire, and W. Gburek (2005), Seasonal ^{18}O variations and groundwater recharge for three landscape types in central Pennsylvania, USA, *J. Hydrol.*, *303*(1–4), 108–124, doi:10.1016/j.jhydrol.2004.08.020.

Queloz, P., L. Carraro, P. Benettin, G. Botter, A. Rinaldo, and E. Bertuzzo (2015), Transport of fluorobenzoate tracers in a vegetated hydrologic control volume: 2. Theoretical inferences and modeling, *Water Resour. Res.*, *51*, 2793–2806, doi:10.1002/2014WR016508.

Renner, M., S. K. Hassler, T. Blume, M. Weiler, A. Hildebrandt, M. Guderle, S. J. Schymanski, and A. Kleidon (2016), Dominant controls of transpiration along a hillslope transect inferred from ecohydrological measurements and thermodynamic limits, *Hydrol. Earth Syst. Sci.*, *20*(5), 2063–2083, doi:10.5194/hess-20-2063-2016.

Schwärzel, K., A. Menzer, F. Clausnitzer, U. Spank, J. Häntzschel, T. Grünwald, B. Köstner, C. Bernhofer, and K.-H. Feger (2009), Soil water content measurements deliver reliable estimates of water fluxes: A comparative study in a beech and a spruce stand in the Tharandt forest (Saxony, Germany), *Agric. For. Meteorol.*, *149*(11), 1994–2006, doi:10.1016/j.agrformet.2009.07.006.

Smith, A., C. Welch, and T. Stadnyk (2016), Assessment of a lumped coupled flow-isotope model in data scarce Boreal catchments, *Hydrol. Processes*, *30*, 3871–3884, doi:10.1002/hyp.10835.

Soulsby, C., C. Birkel, J. Geris, J. Dick, C. Tunaley, and D. Tetzlaff (2015), Stream water age distributions controlled by storage dynamics and nonlinear hydrologic connectivity: Modeling with high-resolution isotope data, *Water Resour. Res.*, *51*, 7759–7776, doi:10.1002/2015WR017888.

Soulsby, C., C. Birkel, and D. Tetzlaff (2016), Characterizing the age distribution of catchment evaporative losses, *Hydrol. Processes*, *30*(8), 1308–1312, doi:10.1002/hyp.10751.

Spence, C. (2006), Hydrological processes and streamflow in a lake dominated watercourse, *Hydrol. Processes*, *20*(17), 3665–3681, doi:10.1002/hyp.6381.

Spence, C., and M.-k. Woo (2003), Hydrology of subarctic Canadian shield: Soil-filled valleys, *J. Hydrol.*, *279*(1–4), 151–166, doi:10.1016/S0022-1694(03)00175-6.

Sprenger, M., B. Herbstritt, and M. Weiler (2015), Established methods and new opportunities for pore water stable isotope analysis, *Hydrol. Processes*, *29*(25), 5174–5192, doi:10.1002/hyp.10643.

Sprenger, M., H. Leistert, K. Gimbel, and M. Weiler (2016a), Illuminating hydrological processes at the soil-vegetation-atmosphere interface with water stable isotopes, *Rev. Geophys.*, *54*(3), 674–704, doi:10.1002/2015RG000515.

Sprenger, M., S. Seeger, T. Blume, and M. Weiler (2016b), Travel times in the vadose zone: Variability in space and time, *Water Resour. Res.*, *52*, 5727–5754, doi:10.1002/2015WR018077.

Tetzlaff, D., C. Soulsby, S. Waldron, I. A. Malcolm, P. J. Bacon, S. M. Dunn, A. Lilly, and A. F. Youngson (2007), Conceptualization of runoff processes using a geographical information system and tracers in a nested mesoscale catchment, *Hydrol. Processes*, *21*(10), 1289–1307, doi:10.1002/Hyp.6309.

Tetzlaff, D., C. Birkel, J. Dick, J. Geris, and C. Soulsby (2014), Storage dynamics in hydropedological units control hillslope connectivity, runoff generation and the evolution of catchment transit time distributions, *Water Resour. Res.*, *50*, 969–985, doi:10.1002/2013WR014147.

Timbe, E., D. Windhorst, P. Crespo, H.-G. Frede, J. Feyen, and L. Breuer (2014), Understanding uncertainties when inferring mean transit times of water trough tracer-based lumped-parameter models in Andean tropical montane cloud forest catchments, *Hydrol. Earth Syst. Sci.*, *18*(4), 1503–1523, doi:10.5194/hess-18-1503-2014.

van Huijgevoort, M. H. J., D. Tetzlaff, E. H. Sutanudjaja, and C. Soulsby (2016), Using high resolution tracer data to constrain water storage, flux and age estimates in a spatially distributed rainfall-runoff model, *Hydrol. Processes*, *30*, 4761–4778, doi:10.1002/hyp.10902.

Yeh, H.-F., C.-H. Lee, and K.-C. Hsu (2011), Oxygen and hydrogen isotopes for the characteristics of groundwater recharge: A case study from the Chih-Pen Creek basin, Taiwan, *Environ. Earth Sci.*, *62*(2), 393–402, doi:10.1007/s12665-010-0534-2.

Zimmermann, U., D. Ehhalt, and K. Münnich (1967), Soil-water movement and evapotranspiration: Changes in the isotopic composition of the water, in *Isotopes in Hydrology*, edited by IAEA, pp. 567–585, Int. At. Energy Agency, Vienna.